International Journal of Psychosocial Rehabilitation, Vol. 24, Issue 08, 2020
ISSN: 1475-7192

Prostate malignant growth Detection utilizing Deep convolutional neural systems

[1]Timmana Hari Krishna, [2]Dr. C. Rajabhushnam

ABSTRACT— *Prostate disease is one of the most well-known types of malignancy and the third driving reason for malignant growth passing in North America. As a coordinated piece of PC supported identification (CAD) devices, dispersion weighted attractive reverberation imaging (DWi) has been seriously read for exact discovery of prostate disease. With profound convolutional neural systems (CNNs) critical accomplishment in PC vision errands, for example, object identification and division, diverse CNN structures are progressively explored in clinical imaging research network as promising answers for planning increasingly exact cAD devices for disease discovery. right now, created and actualized a mechanized CNN-based pipeline for recognition of clinically noteworthy prostate malignant growth (PCa) for a given pivotal DWI picture and for every patient. DWI pictures of 427 patients were utilized as the dataset, which contained 175 patients with PCa and 252 patients without PCa. To gauge the presentation of the proposed pipeline, a test set of 108 (out of 427) patients were saved and not utilized in the preparation stage. The proposed pipeline accomplished region under the recipient working trademark bend (AUC) of 0.87 (95% Confidence Interval (CI): 0.84–0.90) and 0.84 (95% CI: 0.76–0.91) at cut level and patient level, separately.*

Keywords— *Prostate cancer disease, Image Processing, DCNN (Deep Convolutional Neural Network), deep learning pipeline, ResNet*

I. INTRODUCTION

Prostate malignancy is the most widely recognized type of disease among guys in the United States. In 2017, it was the third driving reason for death from disease in men in the United States, with around 161,360 new cases which spoke to 19% of all new malignant growth cases and 26,730 passings, which spoke to 8% of all disease deaths[1]. In spite of the way that prostate malignant growth is the most widely recognized type of disease, whenever distinguished in the beginning periods, the endurance rates are high because of moderate movement of the disease1. In this manner, viable checking and early identification are the key for improved patients' endurance.

Right now, acknowledged clinical strategies to analyze clinically noteworthy prostate malignant growth (PCa) are a blend of the prostate-explicit antigen (PSA) test, computerized rectal test, trans-rectal ultrasound (TRUS), and attractive reverberation imaging (MRI). Be that as it may, PSA screening prompts over-determination, which prompts superfluous costly and excruciating needle biopsies and potential over-treatment[3]. Multiparametric MRI which depends vigorously on dispersion weighted imaging (DWI) has been progressively turning into the standard of care for prostate malignant growth analysis in radiology settings where the zone under the collector working

[1] *Ph.D. Scholar, Computer Science Engineering Department, Bharath Institute of Higher Education and research, Chennai, India, harikrishna.timmana@gmail.com*

[2] *Professor, Computer Science Engineering Department, Bharath Institute of Higher Education and research, Chennai, India, rajabhushanamc.cse@bharathuniv.ac.in*

Received: 21 Dec 2019 | Revised: 18 Jan 2020 | Accepted: 05 Feb 2020

trademark bend (ROC) differs from 0.69 to 0.81 for radiologists identifying PCa3. An institutionalized way to deal with picture translation called PI-RADS v2[5] has been created for radiologists, be that as it may, there remain issues with between spectator fluctuation in the utilization of the PI-RADS scheme5.

Machine Learning is a part of Artificial Intelligence (AI) that depends on the possibility of the framework taking in an example from an enormous scope database by utilizing probabilistic and factual apparatuses and settling on choices or expectations on the new data[7][8][9]. In clinical imaging field, PC helped location and determination (CAD), which is a mix of imaging highlight building and ML order, has indicated potential in helping radiologists for exact finding, diminishing the analysis time and the expense of conclusion. Customary element designing strategies depend on removing quantitative imaging highlights, for example, surface, shape, volume, force, and different factual highlights from imaging information followed by a ML classifier, for example, Support Vector Machines (SVM), Adaboost, and Decision Trees[10][11][12][13][14][15].

Profound learning strategies have demonstrated promising outcomes in an assortment of PC vision assignments, for example, division, arrangement, and item detection[16][17][18]. These strategies comprise of convolution layers that can extricate various highlights from low-level nearby highlights to elevated level worldwide highlights from input pictures. A completely associated layer toward the finish of the convolutional neural layers changes over tangled highlights into the probabilities of certain labels[16]. Various sorts of layers, for example, cluster standardization layer18, which standardizes the contribution of a layer with a zero mean and a unit variation, and dropout layer[20], which is one of regularization strategies that overlooks haphazardly chosen hubs, have been appeared to improve the presentation of profound learning-based techniques. By the by, to accomplish persuading execution, an ideal mixes and structures of the layers just as exact calibrating of hyper-parameters are required[16][18][21]. This remaining parts as one of the principle difficulties of profound learning-based techniques when applied to various fields, for example, clinical imaging. With CNNs' promising outcomes in PC vision field[16][22], the clinical imaging research network has moved their enthusiasm toward profound learning-based techniques for structuring CAD instruments for malignant growth location. As a broadly utilized methodology, the vast majority of proposed calculations require client drawn areas of intrigue (ROI) to order these client explained ROIs to PCa injuries and non PCa sores. Tsehay et al.[23] directed a 3 × 3 pixel level investigation by 5 convolution layers profound VGGNet20 motivated CNN with 196 patients. They tweaked their classifier by cross-approval strategy inside the preparation set with 144 patients and accomplished territory under ROC bend (AUC) of 0.90 AUC on an isolated test set of 52 patients. The outcome depended on 3 × 3 windows of pixels removed from X-ray cuts of DWI, T2-weighted pictures (T2w), and b-esteem pictures of 2000s mm^{-2}.

Le et al.23 led two dimensional (2D) ROI order with mix of melded multimodal Residual Network (ResNet)[18] and the customary carefully assembled highlight extraction strategy. They enlarged the preparation dataset and utilized the test set for calibrating and assessing their classifier. They accomplished ROI-level (injury level) AUC of 0.91. Liu et al.[25] utilized VGGNet motivated 2D CNN classifier to group each example relating to a 32 × 32 ROI (injury) based on biopsy area utilizing a dataset, which was a piece of ProstateX challenge rivalry ("SPIE-AAPM-NCI Prostate MR Classification Challenge")[26]. They isolated the dataset of 341 patients into 3 sets, the preparation set with 199 patients for preparing, approval set with 30 patients for tweaking, and test set with 107 patients for assessment, and applied information growth to every one of the 3 sets. They utilized 4 distinct sorts of information pictures which were produced with various blends of DWI, clear dissemination coefficient

map (ADC), Ktrans from dynamic complexity upgraded attractive reverberation imaging (DCE-MRI), and T2w for their investigation. They accomplished AUC of 0.84 with the increased test.

Mehrtash et al.[27] likewise utilized VGGNet enlivened 9 convolution layers profound three dimensional (3D) CNN classifier to group 3D PCa sores versus non PCa injuries with 32 × 32 × 12 ROI utilizing ADC, high b-esteem pictures, and Ktrans (DCE-MRI) of ProstateX challenge dataset25. They isolated the informational index with 341 patients into preparing set with 201 patients and test set with 140 patients, and accomplished sore level execution of 0.80 AUC on their test set. They applied cross-approval strategy inside the increased preparing set during preparing. As it will be examined in Discussion segment, the proposed strategy right now better analyzed than these ROI-based arrangements as far as strength and relevance in clinical use since it foregoes the requirement for physically or consequently producing ROIs.

Cut level location calculations characterize every MRI cut into with or without PCa tumors. Ishioka et al.[28] played out the cut level investigation with 316 patients by U-Net28 joined with ResNet. They made non-enlarged preparing, approval, and test sets and accomplished AUC of 0.79 on the test set, which included just 17 individual cuts. The proposed calculation right now cut level location also utilizing an a lot bigger example size with better execution analyzed than that proposed by Ishioka et al.[29].

Quiet level calculations order patients into with and without PCa. It is commonly a provoking undertaking to combine ROI-based or cut level outcomes into quiet level results[23][24][25][27][28]. Wang et al.[30] looked at the exhibition of profound learning-based strategies to non-profound learning-put together techniques with respect to the order of PCa MRI cuts versus non PCa MRI cuts with 172 patients. They assessed their VGGNet roused 7 layers (5 convolution layers and 2 inward item layers) CNN classifier's exhibition dependent on cross-approval. Initially, they grouped each cut of a given patient and afterward changed over the cut level outcomes into tolerant level outcomes by a basic democratic system and accomplished the patient-level AUC of 0.84, positive forecast esteem (PPV) of 79%, and negative expectation esteem (NPV) of 77%. Right now, accomplished comparable outcomes with an autonomous test set and bigger example size.

Right now, propose a mechanized pipeline for two degrees of PCa order: cut level and patient level. For cut level order, we have proposed a heap of separately prepared altered ResNet[18] CNNs. We have additionally proposed a novel way to deal with convert cut level arrangement results into tolerant level utilizing first-request measurable highlights extractor, a choice tree-based component selector, and a Random Forest classifier[31][32]. For the strength of the exhibition, we isolated the dataset into three separate sets, the preparation, approval, and test sets, and guaranteed that the test set was never observed by the classifier during preparing and fine-tuning6. We likewise incorporated all cuts that contain prostate and didn't confine the pipeline to cuts that have been chosen for biopsy. Our proposed pipeline's presentation on the autonomous test set was better and more vigorous thought about than comparative examinations that proposed CAD apparatuses for PCa recognition utilizing CNNs.

II. METHODS USED

A. Resource of dataset

An associate of 427 successive patients with a PI-RADS score of 3 or higher who experienced biopsy were incorporated. Out of 427 patients, 175 patients had clinically critical prostate malignant growth and 252 patients didn't. An aggregate of 5,832 2D cuts of each DWI succession (e.g., b0) which contained prostate organ were

utilized as our dataset. We set the patient with Gleason score higher than or equivalent to 7 (International Society of Uropatholgists grade gathering (GG >= 2) as the patient with a clinically critical prostate malignant growth and patient with Gleason score lower than or equivalent to 6 (GG = 1) or with no disease (GG = 0) as the patient without a clinically huge prostate malignant growth.

B. Aquizition

The DWI information was gained between January 2014 to July 2017 utilizing a Philips Achieva 3T entire body unit MR imaging scanner. The transverse plane of DWI successions was gotten utilizing a solitary space turn reverberation planar imaging grouping with four b esteems (0, 100, 400, and 1000s mm^{-2}), redundancy time (TR) 5000~7000 ms, reverberation time (TE) 61ms, cut thickness 3mm, field of view (FOV) 240 mm × 240 mm and network of 140 × 140.

DWI is a MRI arrangement which gauges the affectability of tissue to Brownian movement and it has been seen as a promising imaging strategy for PCa detection [33]. The DWI picture is generally created with various b esteems (0, 100, 400, and 1000s mm^{-2}) which produces different sign powers speaking to the measure of water dispersion in the tissue and can be utilized to evaluate ADC and figure high b-esteem pictures (b1600[33].

So as to utilize DWI pictures as contribution to our profound learning system, we resized the entirety of the DWI cuts into 144 × 144 pixels, and focus trimmed them with 66 × 66 pixels to such an extent that the prostate was secured. The CNNs were changed to take care of DWI information with 6 channels (ADC, b0, b100, b400, b1000, and b1600) rather than pictures with 3 channels (red, green and blue.)

C. Training, validation, and test sets.

We isolated 427 patients DWI pictures into three distinct sets, the preparation set with 271 patients (3,692 cuts), the approval set with 48 patients (654 cuts), and the test set with 108 patients (1,486 cuts) where the preparation/approval/test proportion was 64%, 11%, 25%. The division technique of the dataset was as per the following. In the first place, we isolated the dataset into two sets, the preparation/approval set as 75% and the test set as 25% to keep up a sensible example size for the test set. Second, we isolated the preparation/approval set into two sets with preparing set as 85% of preparing/approval set and the approval set as 15% of preparing/approval set (Table 1). The proportions between the PCa patients and non PCa patients were kept generally comparable all through the informational indexes.

TABLE I. TRAIN,TEST AND VALIDATION DATA SETS OF PATIENT AND SLICES WITH AND WITHOUT PCAS.

x	Patients with PCa	Patients without PCa	Slices with PCa tumors	Slices without PCa tumors
Train dataset	105	166	439	3,253
Test dataset	52	56	226	1260
Validation dataset	18	30	66	588

D. Preprocessing

All of DWI pictures in the dataset were standardized over the whole dataset utilizing the accompanying capacity.

$$X_{i\_normalized} = \frac{X_i - \mu}{std}$$

where X_i is the pixels in an individual MRI cut, μ is the mean of the dataset, sexually transmitted disease is the standard deviation of the dataset, and $X_{i\_normalized}$ is the standardized individual MRI cut.

E. Pipeline

The proposed pipeline comprises of three phases. In the main stage, each DWI cut is arranged utilizing five independently prepared CNNs models. In the subsequent stage, first-request factual highlights (e.g., mean, standard deviation, middle, and so on.) are extricated from the likelihood sets of CNNs yields, and significant highlights are chosen through a choice tree-based component selector. In the last stage, a Random Forest classifier is utilized to characterize patients into bunches with and without PCa utilizing these first request factual highlights. The Random Forest classifier was prepared and calibrated by the highlights extricated from the approval set with 10 crease cross-approval technique.

F. ResNet

Since ResNet design has demonstrated promising execution in numerous PC vision tasks [18], we picked it as our base engineering for this examination. Every Residual Block comprises of convolutional layers [22] and personality easy route connection [18] that avoids those layers, and their results are included toward the end, as appeared in Figure 1-a. At the point when information and yield measurements are the equivalent, the personality alternate routes, meant by x, can be legitimately applied. The accompanying equation shows the character mapping process.

$$b = F(a, \{W_i\}) + a \qquad (2)$$

where $F(a, \{W_i\})$ is the yield from convolutional layers and a is the information. At the point when the element of info isn't equivalent to that of the yield (e.g., toward the finish of the Residual Block), the straight projection W_s changes the element of the contribution to be same as that of the yield which is characterized as:

$$b = F(a, \{W_i\}) + W_s a \qquad (3)$$

To improve the presentation of the design, we executed a completely pre-initiated leftover network[35]. In the first ResNet, cluster standardization and ReLU actuation layers were trailed the convolution layer, however in pre-initiation ResNet, bunch standardization and ReLU enactment layers precedes the convolution layers. The upside of this structure is that the angle of a layer doesn't evaporate in any event, when the loads are discretionarily small[34]. Rather than 2-layer profound ResNet square, we executed a 3-layer profound "bottleneck" building obstruct since it essentially diminishes preparing time without giving up the performance[18] (Figure 1-b).

G. CNN Architecture and Training

A 41 layers profound ResNet was made for the cut level order. The engineering is made out of 2D convolutional layers with a 7 × 7 channel followed by a 3 × 3 Max pooling layer and remaining squares (Res Block). The profundity of 41 layers were seen as ideal through hyper-parameter adjusting technique utilizing the approval set. Since the information pictures were little (66 × 66 pixels) and the tumorous locales were considerably littler (e.g., 4 × 3 pixels), extra ResNet squares or more profound systems were required. The first ResNet Block (ResNet Block1 in Table 2) is 3-layer bottleneck obstructs with 2D CNN layers with channel sizes 64, 64 and 256 which is stacked multiple times. The second ResNet Block (ResNet Block2 in Table 2) is 3-layer bottleneck obstructs with

2D CNN layers with channel sizes 128, 128, and 512 which is stacked multiple times. 2 × 2 2D Average Pooling, Dropout layer, and 2D Fully associated Layer with 1000 hubs for two probabilistic yields are trailed before the finish of Res Blocks. Table 2 shows the review of the proposed CNNs design. Stochastic Gradient Decent35 was utilized as the enhancer with the underlying learning pace of 0.001, and it was decreased by a factor of 10 when the model quit improving after cycles. The model was prepared with the clump size set to 8. Dropout rate was set to 0.90. We utilized a weight rot of 0.000001 and an energy of 0.90. Since the dataset is amazingly unequal, twofold cross entropy36 was utilized as the misfortune work.

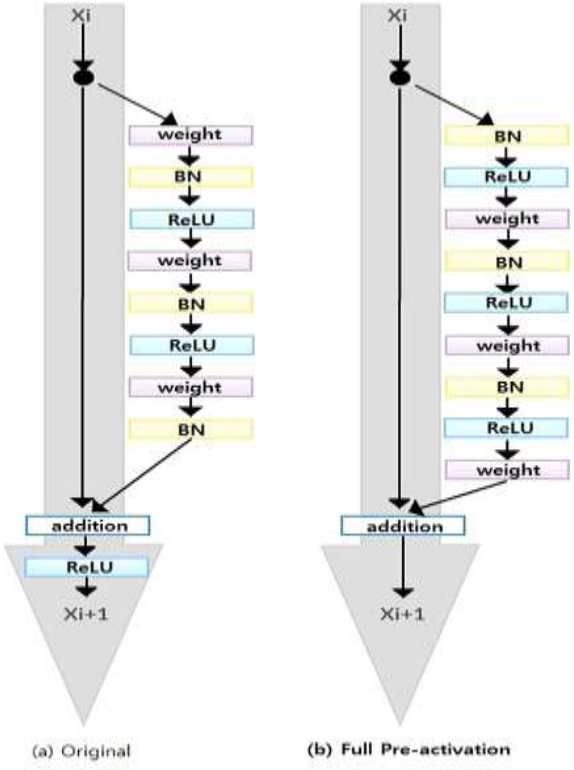

Fig. 1. Architectureal differece between original and activated ResNet

H. Stacked Speculation

Because of the irregularity in preparing CNNs (for example, toward the start of preparing CNNs, loads are set to subjective arbitrary numbers), each CNN might be diverse in spite of indistinguishable arrangement of hyper-parameters and info datasets. This implies each CNN may catch various highlights for the patient-level arrangement. Stacked generalization [38] is a gathering system that prepares numerous classifiers with the equivalent dataset and makes a last forecast utilizing a blend of individual classifiers' expectations. Stacked speculation regularly yields better order execution contrasted with a solitary classifier37. We actualized a straightforward stacked speculation strategy utilizing five CNNs. The quantity of stacked CNNs was chosen dependent on the best execution and expanding the quantity of CNNs didn't show enhancement for the patient-level execution. Since there is a restricted example size for persistent level (48 patients for approval, which was utilized to prepare Random Forest classifier for quiet level discovery), expanding the quantity of CNNs, which prompts an expanded number of patient-level highlights (as examined in the following area), improves the probability of overfitting and henceforth, diminishes the model's robustness38. All the cut level probabilities produced by the five CNNs were taken care of into a first-request measurable highlights extractor to create one lot

of highlights for every patient. In the proposed pipeline, the patient-level execution fundamentally improved (2-followed P = 0.048) utilizing five CNNs contrasted with a solitary CNN (AUC: 0.84, CI: 0.76–0.91, versus AUC: 0.71, CI: 0.61–0.81).

I. First order statistical feature extraction

Leave p_{ij} and n_{ij} alone the probabilities of a MRI cut related with PCa and non PCa, separately, where I speaks to one of five independently prepared CNNs and j speaks to every MRI cut of a patient. Each CNN produces two likelihood sets, $P_i = \{p_{i1}, p_{i2}, \dots, p_{iN}\}$ and $N_i = \{n_{i1}, n_{i2}, \dots, n_{iN}\}$ where N is the absolute number of MRI cuts for every patient. Inside the likelihood sets, top five probabilities which are higher than 0.74 were chosen (P_i' and N_i'). This was done to guarantee less important probabilities at cut level were not utilized for patient-level classification. The likelihood cut-off of 0.74 was chosen by lattice search utilizing the approval set. dislikes the absolute number of factual highlights, were removed for every patient. Next, the significant highlights, Next, from the new likelihood sets, P_i' and N_i', the main request measurable highlights set, $F_i = \{f_{i1}, f_{i2}, \dots, f_{ik}\}$ where K rep-

TABLE II. PROPOSED CNN ARCHITECTURE

Layer Name	Layer Details
Conv layer	2D Convolutional Layer (7 ×× 7, 64, stride 2)
Max Pool	3 × 3 max pool, stride
ResNet Block 1	$\begin{bmatrix} 1 \times 1,64 \\ 3 \times 3,64 \\ 1 \times 1,256 \end{bmatrix}$ x4
ResNet Block 2	$\begin{bmatrix} 1 \times 1,128 \\ 3 \times 3,128 \\ 1 \times 1,512 \end{bmatrix}$ x9
Ave Pool	2D Average Pooling (7 ×× 7)
FC	Fully Connected Layer (2D, softmax)

F_i were chosen by a choice tree-based component selector [40]. The last list of capabilities was built by consolidating significant highlights, Fí, for each of the five CNNs where $F_i = \{f_1, f_2, \dots, f_k\}$.

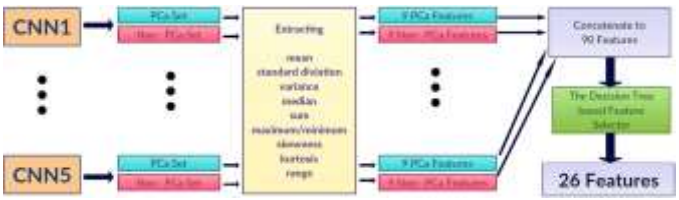

Fig. 2. Proposed first order feature extracter

We extricated nine first-request highlights which are the mean, standard deviation, difference, middle, aggregate, least (just from non PCa class), greatest (just from PCa class), skewness40, kurtosis40, and extend from the base to most extreme from every likelihood set. This created 90 highlights for every patient (9 highlights for PCa and 9 highlights for non PCa class for each CNN). We chose 26 best highlights utilizing the choice tree-based

component selector[40]. The choice tree based-include selector was calibrated and prepared with 10 overlay cross-approval technique utilizing the validation set (Fig. 2). When first-request factual highlights were separated for every patient, a Random Forest classifier30,31 was prepared utilizing the approval set and tried on the test set for persistent level grouping.

The CNNs were prepared utilizing one Nvidia Titan X GPU, 8 centres Intel i7 CPU and 32 GB memory. It took 6 hours to prepare every one of the five CNNs with up to 100 emphases, under 10 seconds to prepare the Random Forest classifier, and under 1 moment to test each of the 108 patients.

III. RESULTS

The AUC and ROC curve41 were utilized to assess the exhibition of the proposed pipeline. A ROC bend is a generally utilized strategy to envision the exhibition of a twofold classifier by plotting genuine positive rates and bogus positive rates with various limits, and an AUC outlines its presentation with a solitary number. The extraordinary bit of leeway of AUC is its legitimacy in an uneven dataset. Since just few DWI cuts have PCa tumor (e.g., normal of 1 to 3 cuts for each patient where the complete number of cuts are a normal of 14), AUC is the most ideal approach to assess the exhibition of the pipeline. Likewise, ROC bend permits us to pick wanted explicitness as well as affectability of the classifier through the edge. This assessment technique is applied to cut level and patient-level arrangements utilizing the test set with 108 patients (1,486 cuts).

Slice level execution: Since the pipeline contains five exclusively prepared CNNs, there are five distinctive test results at cut level. Table 3 shows singular execution on the test set for each CNN. Our best CNN (CNN1) accomplished the DWI cut level AUC of 0.87 (95% Confidence Interval (CI): 0.84–0.90). Figure 3 shows the ROC bend of CNN1 execution.

Patient level execution: The patient-level AUC by our Random Forest classifier with the highlights removed through CNNs was 0.84 (95% CI: 0.76–0.91) (Fig. 4).

IV. DISCUSSION

In the writing, a few PCa grouping strategies for MRI pictures have been created to address the inalienable difficulties of CAD instruments for disease location, which can be classified into two classes: radiomics-driven element based methods[10][11][12][13][43][44] and profound learning-based methods[23][24][25][27][28][30].

Radiomics-driven component-based techniques comprise of two phases: extraction of handmade highlights and characterization dependent on these highlights. These techniques require an exhaustive arrangement of radiomic highlights, which incorporate first-and second-request measurable highlights, elevated level highlights, for example, morphological features [10], and voxel-level features [11]. For the arrangement utilizing radiomic highlights, a few methodologies have been proposed. Distinctive AI classifiers [7], for example, guileless Bayesian classifier [10], SVM[43][44], and Random Forest classifier[11] have been utilized. Notwithstanding, it has been indicated that profound learning strategies are better than radiomics-driven element-based techniques in order of PCa[30].

return for capital invested is one of generally utilized information structures in clinical picture examination. Normally outlined by the client, ROIs are tests inside clinical pictures recognized for a specific purpose [45], which frequently contain malignant growth tumors. return on initial capital investment-based techniques legitimately look at and just order locales or jumping boxes that contains tumors over sound tissues. return for capital invested based techniques have been utilized in both radiomics-driven and CNN-based strategies for PCa CAD apparatus plan. In CNN-based strategies, Liu et al[25], Tsehay et al. [23], and Le et al. [24] utilized 2D ROIs of malignant growth tumors and Mehrtash et al. [27] and utilized 3D ROIs of disease tumors as their information structures (eg. 32 × 32 × 12 ROI).

return on initial capital investment-based CAD calculations have a few impediments. To begin with, ROI-based calculations require a tedious physically created (by master peruser) or naturally produced division of ROI as a piece of the pipeline to create ROI-based dataset. In the event that it is a physically produced division, the application for clinical use is restricted on the grounds that it at last depends on the clinician's survey and aptitude and subsequently, it isn't completely computerized. On the off chance that, then again, it is a consequently created division, the consequence of characterization relies upon the exhibition of the division calculation, and mistakes from ROI division calculation can prompt poor PCa recognition execution.ROI-based methods [23][25][27] battle to consolidate singular ROI-based outcomes into understanding level arrangement and they generally depend on fundamental blending strategies, for example, straightforward voting[30], which makes it a provoking assignment to accomplish adequate execution at quiet level.

Right now, of taking care of ROIs into CNNs, we utilized consequently focus edited DWI pictures with the main client mediation being to show the first and last cut that contained prostate organ. Proposed pipeline execution is free of ROI age technique. As it were, our pipeline can perform PCa conclusion on patients without the guide of master perusers. A comparative methodology was taken by Liu et al. [25] where 32 × 32 ROIs were built around biopsy areas. The primary contrast between this methodology and our own is that in the previous, just cuts with biopsy were utilized and the staying of cuts, which are most of them, were avoided from the model. In our pipeline, we fabricated the ROI around the prostate with no from the earlier information on the biopsy areas, which makes our methodology autonomous of radiologists. In spite of the fact that the outcome for Liu et al. approach24 was accounted for increased test set and just for cuts with biopsy, our pipeline AUC was unrivalled (AUC of 0.87 versus 0.84).

There are different investigations in the writing that proposed cut based analysis27,29, however our cut level presentation (AUC: 0.87) and the example size of the test set (108 patients or 1,486 cuts), were fundamentally better than their exhibition and test size. For instance, Ishioka et al.27 proposed a cut level calculation utilizing 316 patient information for preparing and approval. The test set was just 17 cuts withe AUC of 0.79. Moreover, we utilized the outcomes produced by CNNs as highlights for grouping PCa at understanding level, which was not the situation with these past takes a shot at cut level calculations.

Totally detaching test information from preparing and approval is significant to gauge genuine execution of a (profound) AI based classifier. Cross-approval is a notable technique to assess the exhibition of the classifier [30].Adjusting the classifier dependent on the presentation of the test set (e.g., received in [24]) makes the test set not autonomous from the prepared and upgraded classifier, and consequently, the exhibition accomplished is hopeful and not sensible. The calibrating and streamlining of the model must be done through an approval set,

which is discrete than both preparing and test sets as received in our work right now those of [23][27][28]. Because of test information cross-sullying with preparing or approval sets by means of cross-approval or information growth, the presentation of a portion of the proposed models in the writing is somewhat hopeful.

Right now, partitioned the whole dataset into three unique sets, preparing, approval, and test set. In the cut level examination, the preparation set was utilized to prepare the model, and the approval set was utilized to adjust and upgrade our CNNs design, and the test set was utilized to assess the exhibition of the CNNs. In the patient-level examination, cross approval was utilized inside the approval set to tweak and enhance our choice tree-based component selector and Random Forest classifier, and tried on the test set. Therefore, our classifier's outcomes were progressively strong contrasted with considers that pre-owned cross-approval as a proportion of performance [30] or preparing profound learning classifier without the validation set [24]. For the examinations that pre-owned free test set [25][27][28], our outcomes are prevalent. For instance, Liu et al.24 directed 2D ROI cut level examination and accomplished 0.84 AUC for ROC (based on biopsy area) order just contrasted with 0.87 AUC for our proposed pipeline for cut level grouping.

Turning ROI-level outcomes or the cut level aftereffects of MRI information into understanding level outcome has been a significant test in PCa order by means of profound learning [23][24][25][27][28]. This is because of the way that the 3D MRI volume of every patient may have hundreds or thousands of ROIs. Wang et al. [30] changed over their cut level outcome into understanding level by averaging the entirety of the cut level probabilities for tolerant and thresholding the normal probabilities to characterize PCa at quiet level. In spite of the fact that this technique accomplished patient-level execution like our proposed pipeline's outcomes (AUC: 0.84), it depends on cross approval, which makes it a hopeful outcome. Interestingly, the outcomes introduced right now dependent on a test set which is totally discrete than the preparation and approval sets. In addition, our test information contained 108 patients, which is essentially bigger than the dataset with 17 patients for each fold [30].

The fundamental confinement of this work is the way that like CAD papers, the information is naturally one-sided; those patients are sent to MRI who have a sign of prostate disease (e.g., higher PSA). Consequently, the dataset is definitely not a genuine impression of the populace. Furthermore, the marks for the information depend on biopsy areas, which are dictated by radiologists. As it were, cuts with no biopsy are thought to be negative, in view of radiology reports. Notwithstanding, the positive cuts depend on pathology (biopsy) reports. At long last, an outside approval with a dataset from an alternate foundation is required to check the exhibition and heartiness of the proposed pipeline across scanners and organizations.

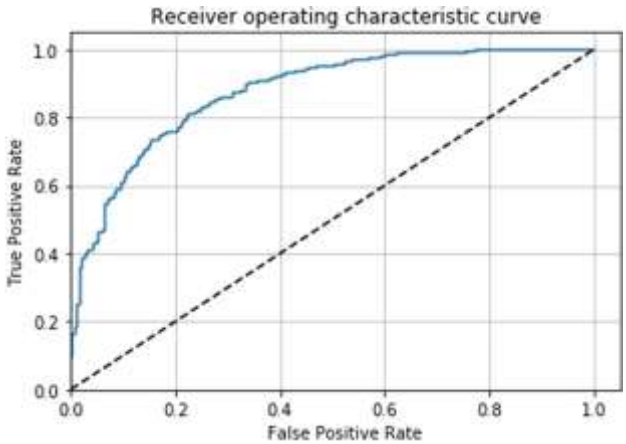

Fig. 3. Slice-level ROC curve

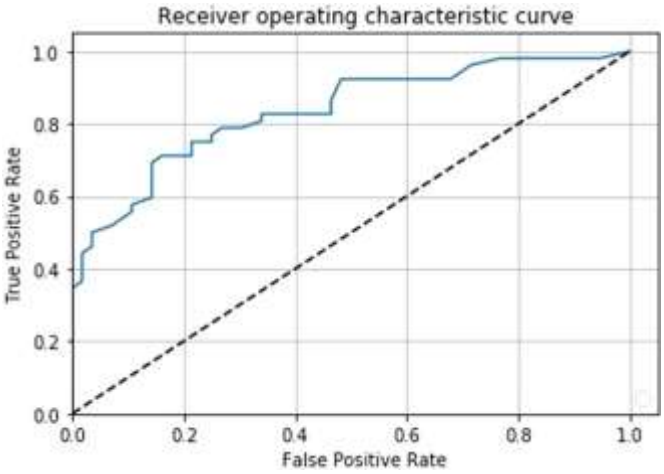

Fig. 4. Patient Level ROC Curve

V. CONCLUSION

Right now, constructed a two-stage computerized profound learning pipeline for cut level and patient-level PCa finding utilizing DWI pictures. Rather than manual ROI explanation, robotized focus trimming was utilized to keep up freedom from master perusers' mediation. A heap of five CNNs were utilized to create improved arrangement results at cut level. First-request measurable highlights were extricated from cut level probabilities to incorporate cut level characterization results into quiet level. The pipeline was tried on an autonomous test set of 108 patients and the outcomes at both cut level and patient level was better than the cutting edge. As future work, other CNN structures, for example, 3D CNNs (to take care of the 3D DWI) and repetitive neural networks [46] (to represent sequentiallity of injuries in neighboring cuts) will be utilized

REFERENCES

1. Siegel, R. L., Miller, K. D. & Jemal, A. Cancer statistics, 2017. CA: a cancer journal for clinicians **67**, 7–30 (2017).
2. Hari Krishna, Timmana, Detection of mammographic cancer using support vector machine and deep neural network. Journal of mechanics of continua and mathematical sciences 2019, vol.8 doi: 14. 10.26782/jmcms.2019.12.00013.
3. Sandhu, G. S. & Andriole, G. L. Overdiagnosis of prostate cancer. Journal of the National Cancer Institute Monographs **2012**, 146–151 (2012).
4. Sonn, G.A.et al. Prostate magnetic resonance imaging interpretation varies substantially across radiologists. Eur. urology focus (2017).
5. Hassanzadeh, E.et al. Prostate Imaging Reporting and Data System Version 2 (PIRADS v2): A pictorial review. Abdom Radiol **42**, 278–289 https://doi.org/10.1016/j.trsl.2014.08.005. (2017).
6. Rosenkrantz, A. B. et al. Interobserver reproducibility of the pi-rads version 2 lexicon: a multicenter study of six experienced prostate radiologists. Radiology **280**, 793–804 (2016).
7. Nasrabadi, N. M. Pattern recognition and machine learning. Journal of electronic imaging **16**, 049901 (2007).

Received: 21 Dec 2019 | Revised: 18 Jan 2020 | Accepted: 05 Feb 2020

8. Goldberg, D. E. & Holland, J. H. Genetic algorithms and machine learning. Machine learning **3**, 95–99 (1988).
9. Michalski, R. S., Carbonell, J. G. & Mitchell, T. M. Machine learning: An artificial intelligence approach (Springer Science & Business Media, 2013).
10. Cameron, A., Khalvati, F., Haider, M. A. & Wong, A. Maps: a quantitative radiomics approach for prostate cancer detection. IEEE Transactions on Biomed. Eng. **63**, 1145–1156 (2016).
11. Litjens, G., Debats, O., Barentsz, J., Karssemeijer, N. & Huisman, H. Computer-aided detection of prostate cancer in mri. IEEE transactions on medical imaging **33**, 1083–1092 (2014).
12. Wang, S., Burtt, K., Turkbey, B., Choyke, P. & Summers, R.M.Computer aided-diagnosis of prostate cancer on multiparametric mri: a technical review of current research. BioMed research international **2014** (2014).
13. Fehr, D. et al. Automatic classification of prostate cancer gleason scores from multiparametric magnetic resonance images. Proc. of the Natl. Acad. of Sci. **112**, E6265–E6273 (2015).
14. Erickson, B. J., Korfiatis, P., Akkus, Z. & Kline, T. L. Machine learning for medical imaging. Radiographics **37**, 505–515 (2017).
15. Orru, G., Pettersson-Yeo, W., Marquand, A. F., Sartori, G. & Mechelli, A. Using support vector machine to identify imaging biomarkers of neurological and psychiatric disease: a critical review. Neurosci. & Biobehav. Rev. **36**, 1140–1152 (2012).
16. Krizhevsky, A., Sutskever, I. & Hinton, G.E. Imagenet classification with deep convolutional neural networks. In Advances in neural information processing systems, 1097– 1105 (2012).
17. Long, J., Shelhamer, E. & Darrell, T.Fully convolutional networks for semantic segmentation. In Proceedings of the IEEE conference on computer vision and pattern recognition, 3431– 3440 (2015).
18. He, K., Zhang, X., Ren, S. & Sun, J. Deep residual learning for image recognition. In Proceedings of the IEEE conference on computer vision and pattern recognition, 770– 778 (2016).
19. Ioffe, S. & Szegedy, C. Batch normalization: Accelerating deep network training by reducing internal covariate shift. arXiv preprint arXiv:1502.03167 (2015).
20. LeCun, Y., Bengio, Y. & Hinton, G. Deep learning. nature **521**, 436 (2015).
21. Simonyan, K. & Zisserman, A. Very deep convolutional networks for large-scale image recognition. arXiv preprint arXiv:1409.1556 (2014).
22. LeCun, Y., Bengio, Y. & Hinton, G. Deep learning. nature **521**, 436 (2015).
23. Tsehay, Y.et al. Biopsy-guided learning with deep convolutional neural networks for prostate cancer detection on multiparametric mri. In Biomedical Imaging (ISBI 2017), 2017 IEEE 14th International Symposium on, 642– 645 (IEEE, 2017).
24. Le, M. H. et al. Automated diagnosis of prostate cancer in multi-parametric mri based on multimodal convolutional neural networks. Phy. in Medicine & Bio. **62**, 6497 (2017).
25. Liu, S., Zheng, H., Feng, Y. & Li, W. Prostate cancer diagnosis using deep learning with 3d multiparametric mri. In Medical Imaging 2017: Computer-Aided Diagnosis, vol. 10134, 1013428 (International Society for Optics and Photonics, 2017).
26. Armato, S. G., Petrick, N. A. & Drukker, K.Prostatex: Prostate mr classification challenge (conference presentation). Proceedings of the SPIE, Volume 10134, id. 101344G 1 pp.(2017).**134** (2017).

27. Mehrtash, A.et al. Classification of clinical significance of mri prostate findings using 3d convolutional neural networks. In Medical Imaging 2017: Computer-Aided Diagnosis, vol. 10134, 101342A (International Society for Optics and Photonics, 2017).
28. Ishioka, J. et al. Mp20-10 deep learning with a convolutional neural network algorithm for fully automated detection of prostate cancer using pre-biopsy mri. The Journal of Urology **199**, e256 (2018).
29. Ronneberger, O., Fischer, P. & Brox, T. U-net: Convolutional networks for biomedical image segmentation. In International Conference on Medical image computing and computer-assisted intervention, 234– 241 (Springer, 2015).
30. Wang, X. et al. Searching for prostate cancer by fully automated magnetic resonance imaging classification: deep learning versus non-deep learning. Sci. reports **7**, 15415 (2017).
31. Breiman, L. Random forests. Machine learning **45**, 5–32 (2001).
32. Nguyen, C., Wang, Y. & Nguyen, H. N. Random forest classifier combined with feature selection for breast cancer diagnosis and prognostic. J. of Biomed. Sci. and Eng. **6**, 551 (2013).
33. Padhani, A. R. et al. Diffusion-weighted magnetic resonance imaging as a cancer biomarker: consensus and recommendations. Neoplasia **11**, 102–125 (2009).
34. Glaister, J., Cameron, A., Wong, A. & Haider, M.A. Quantitative investigative analysis of tumour separability in the prostate gland using ultra-high b-value computed diffusion imaging. In Engineering in Medicine and Biology Society (EMBC), 2012 Annual International Conference of the IEEE, 420– 423 (IEEE, 2012).
35. He, K., Zhang, X., Ren, S. & Sun, J. Identity mappings in deep residual networks. In European conference on computer vision, 630– 645 (Springer, 2016).
36. Bottou, L. Large-scale machine learning with stochastic gradient descent. In Proceedings of COMPSTAT'2010, 177– 186 (Springer, 2010).
37. De Boer, P.-T., Kroese, D. P., Mannor, S. & Rubinstein, R. Y. A tutorial on the cross-entropy method. Annals of operations research **134**, 19–67 (2005).
38. Wolpert, D. H. Stacked generalization. Neural networks **5**, 241–259 (1992).
39. Vapnik, V.The nature of statistical learning theory (Springer science and business media, 2013).
40. Saeys, Y., Inza, I. & Larrañaga, P. A review of feature selection techniques in bioinformatics. bioinformatics **23**, 2507–2517 (2007).
41. Kim, H.-Y. Statistical notes for clinical researchers: assessing normal distribution (2) using skewness and kurtosis. Restorative dentistry & endodontics **38**, 52–54 (2013).
42. Hanley, J. A. & McNeil, B. J. The meaning and use of the area under a receiver operating characteristic (roc) curve. Radiology **143**, 29–36 (1982).
43. Khalvati, F., Wong, A. & Haider, M. A. Automated prostate cancer detection via comprehensive multi-parametric magnetic resonance imaging texture feature models. BMC medical imaging **15**, 27 (2015).
44. Khalvati, F. et al. Mpcad: a multi-scale radiomics-driven framework for automated prostate cancer localization and detection. BMC medical imaging **18**, 16 (2018).
45. Brinkmann, R.The art and science of digital compositing: Techniques for visual effects, animation and motion graphics (Morgan Kaufmann, 2008).

46. Mikolov, T., Karafiát, M., Burget, L., Černocky, J. & Khudanpur, S. Recurrent neural network based language model. In Eleventh annual conference of the international speech communication association (2010).